Hydrol. Earth Syst. Sci. Discuss., 11, 5859–5903, 2014
www.hydrol-earth-syst-sci-discuss.net/11/5859/2014/
doi:10.5194/hessd-11-5859-2014

Hydrology and Earth System Sciences
Open Access
Discussions

Monitoring hillslope moisture dynamics with surface ERT and hydrometric point measurement: a case study from Ore Mountains, Germany

R. Hübner[1], K. Heller[1], T. Günther[2], and A. Kleber[1]

[1]Institute of Geography, Dresden University of Technology, Helmholtzstr. 10, 01069 Dresden, Germany
[2]Leibniz Institute for Applied Geophysics (LIAG), Stilleweg 2, 30655 Hannover, Germany

Received: 9 May 2014 – Accepted: 14 May 2014 – Published: 5 June 2014

Correspondence to: R. Hübner (rico.huebner@tu-dresden.de)

Published by Copernicus Publications on behalf of the European Geosciences Union.

Abstract

Hillslopes are one of the basic units that mainly control water movement and flow pathways within catchments. The structure of their shallow subsurface affects water balance, e.g. infiltration, retention, and runoff. Nevertheless, there is still a gap of knowledge of the hydrological dynamics on hillslopes, notably due to the lack of generalization and transferability.

To improve the knowledge of hydrological responses on hillslopes with periglacial cover beds, hydrometrical measurements have been carried out on a small spring catchment in the eastern Ore Mountains since November 2007.

In addition, surface ERT measurements of several profiles were applied to enhance resolution of punctual hydrometric data. From May to December 2008 geoelectrical monitoring in nearly weekly intervals was implemented to trace seasonal moisture dynamics on the hillslope scale. To obtain the link between water content and resistivity, the parameters of Archie's law were determined using different core samples. To optimize inversion parameters and methods, the derived spatial and temporal water content distribution was compared to tensiometer data and resulting in remarkable coincidence. The measured resistivity shows a close correlation with precipitation. Depending on the amount and intensity of rain, different depths were affected by seepage water. Three different types of response to different amounts of precipitation (small, medium, high), could be differentiated. A period with a small amount causes a short interruption of the drying pattern at the surface in summer, whereas a medium amount induces a distinctive reaction at shallow depth (< 0.9 m), and a high amount results in a strong response reaching down to 2 m.

HESSD

11, 5859–5903, 2014

1 Introduction

The knowledge of system-internal water flow pathways and the response to precipitation on different spatial and temporal scales is essential for the prediction of hydrological and hydrochemical dynamics within catchments (Uhlenbrook et al., 2008; Wenninger et al., 2004). Understanding the involved processes is of particular importance for improving precipitation-runoff and pollutant-transport models (Di Baldassarre and Uhlenbrook, 2012).

The hillslopes are an important link between the atmosphere and the water input into catchments, and they mainly control different runoff components and residence times (Uhlenbrook et al., 2008). Several studies have addressed hillslope hydrology (Anderson and Burt, 1990; Kirkby, 1980; Kleber and Schellenberger, 1998; McDonnell et al., 2001; Tromp-van Meerveld, 2004; Uchida et al., 2006). A major problem is that the spatial and temporal variability of the hydrological response due to different natural settings – e.g. geomorphological, pedological, lithological characteristics and the spatial heterogeneity – make it difficult to generalize and to transfer results to ungauged basins (McDonnell et al., 2007).

In catchments of Central European subdued mountain range, the shallow subsurface of hillslopes is mostly covered by Pleistocene periglacial slope deposits (Kleber and Terhorst, 2013). These up to three layered cover beds (Upper Layer – LH, Intermediate Layer – LM, Basal Layer – LB: classification according to AD-hoc AG-Boden, 2005; Kleber and Terhorst, 2013), have different regional and local characteristics and remarkable influence on water budgets as well as on water fluxes. Due to the sedimentological and substrate-specific properties, e.g. grain size distribution, clast content, and texture, they are of particular importance for near surface runoff as well as for interflow (Chifflard et al., 2008; Kleber, 2004; Kleber and Schellenberger, 1998; Sauer et al., 2001; Scholten, 1999; Völkel et al., 2002a, b; Heller, 2012; Moldenhauer et al., 2013).

HESSD
11, 5859–5903, 2014

Most of the implemented studies were based on invasive and expansive hydrometric point measurements on the punctual scale or on tracer investigation, which integrates entire catchments. Due to the lack of direct measurements on an intermediate (hillslope) scale and considering the existing complexities and spatio-temporal interlinking of near-surface processes and groundwater dynamics, there is still a lack of knowledge regarding runoff generation in watersheds (McDonnell, 2003; Tilch et al., 2006; Uhlenbrook, 2005). Additional methods are needed to improve the understanding of these complex processes, especially at the hillslope scale. Hydrogeophysical methods are capable of closing the gap between large-scale depth-limited remote-sensing methods and invasive punctual hydrometric arrays (Robinson et al., 2008a, b; Lesmes and Friedman, 2006; Uhlenbrook et al., 2008).

Many studies show the potential of ERT for hydrological investigation by means of synthetic case studies for aquifer transport characterization (Kemna et al., 2004; Vanderborght et al., 2005), imaging water flow on soil cores (Bechtold et al., 2012; Binley et al., 1996a, b; Garré et al., 2011, 2010; Koestel et al., 2009a, b, 2008), cross borehole imaging of tracers (Daily et al., 1992; Oldenborger et al., 2007; Ramirez et al., 1993; Singha and Gorelick, 2005; Slater et al., 2000), or imaging of tracers or irrigations with surface ERT (Cassiani et al., 2006; De Morais et al., 2008; Descloitres et al., 2008a; Michot et al., 2003; Perri et al., 2012). However, some research has been conducted under natural conditions to characterize water content change, infiltration or discharge by use of cross borehole ERT (French and Binley, 2004), surface ERT (Brunet et al., 2010; Benderitter and Schott, 1999; Descloitres et al., 2008b; Massuel et al., 2006; Miller et al., 2008) or a combined surface cross-borehole ERT array (Beff et al., 2013; Zhou et al., 2001).

Beside hydrogeophysical methods such as EM (Popp et al., 2013; Robinson et al., 2012; Tromp-van Meerveld and McDonnell, 2009), time-lapse ERT has been frequently applied to hillslope investigation in the runoff and interflow (Uhlenbrook et al., 2008; Cassiani et al., 2009) or preferential flow context (Leslie and Heinse, 2013). However,

HESSD
11, 5859–5903, 2014

the use of ERT for mapping shallow subsurface structures and monitoring hydrological dynamics on hillslopes is still uncommon.

The objective of this paper is to show the potential of non-invasive surface ERT for mapping the spatial heterogeneities of shallow subsurface structures on a hillslope with periglacial cover beds. Furthermore, we used time-tapse ERT to monitor long-term soil moisture dynamics to improve the spatial resolution of additional hydrometric measurements (e.g. tensiometer and FDR-Sensors). With this multi method approach, we tried to achieve a better understanding of the influence of the layered subsurface on different runoff components and the response to different amounts of precipitation on hillslopes.

2 Material and methods

2.1 Study site

The study area covers the 6 ha of a forested spring catchment in the Eastern Ore Mountains, eastern Germany, which is located in the Freiberger Mulde catchment (Fig. 1). Annual precipitation averages 930 mm, mean annual temperature is 6.6 °C. The altitude ranges from 521 to 575 m a.s.l. The catchment is formed as a slope hollow with a mean slope inclination of approximately 7°. Bedrock is gneiss overlain by periglacial cover beds with up to three layers (Heller, 2012). The upper layer (LH) with a thickness of 0.3 to 0.65 m consists of silty-loamy material with a low bulk density and many roots (cf. Table 1). In the central part of the slope hollow, a silty-loamy intermediate layer (LM) follows with higher bulk density and a thickness of up to 0.55 m. The ubiquitous sandy-loamy basal layer (LB) is characterized by even higher bulk density and coarse clasts oriented parallel to the slope. Down slope it may reach a thickness of at least 3 m (cf. Fig. 1).

HESSD
11, 5859–5903, 2014

2.2 Hydrometrical equipment

Since November 2007 soil water tension has been measured using 76 recording tensiometers (UMS – T8, 10 min intervals) arranged in 14 survey points along the slope at 5 to 7 different depths (cf. Fig. 1). Additionally, at the survey point H3a five ThetaProbes (FDR-Sensors – Delta T devices – ML2x) were installed to measure volumetric water content. A V-notch weir with a pressure meter was used to quantify spring discharge. Rainfall was recorded by 4 precipitation gauges with tipping bucket. For determination of pore water conductivity and resistivity, soil water was extracted with suction cups (VS-pro Vakuum System Co. UMS) at four depths at three locations (S1, S2, S3; Fig. 1) and cumulated as a weekly mixed sample.

2.3 Laboratory work

Quality, amount, and distribution of pore water exert a huge influence on resistivity and form the link between electrical and hydrological properties. The empirical relationship of Archie's law (Archie, 1942) describes the connection between electrical resistivity and saturation in porous media. Instead of saturation we use the volumetric water content Θ with:

$$\rho_{\text{eff}} = F_{\Theta}\rho_{\text{w}}\Theta^{-n_{\Theta}} \tag{1}$$

where ρ_{eff} is the bulk resistivity of the soil probe and ρ_{w} is the resistivity of the pore fluid. The formation factor F_{Θ} describes the increase of resistivity due to an isolating solid matrix and constitutes an intrinsic measure of material microgeometry (Schön, 2004; Lesmes and Friedman, 2006). The exponent n_{Θ} is an empirical constant, which depends on the distribution of water within the pore space (Schön, 2004).

This model disregards the surface conductivity, which may occur due to interactions between pore water and soil matrix, especially with a high percentage of small grain sizes. In our study the curve fitting could be carried out very well without considering this, thus it was not taken into account.

HESSD
11, 5859–5903, 2014

To investigate the petrophysical relationship between resistivity and water content, 15 undisturbed soil core specimens (diameter = 36 mm, length = 40 mm) taken at different depths (0.3 to 1.4 m) were analyzed. After dehydration in a drying chamber, the samples were saturated successively. Using a 4-point array, electrical resistivity was measured for different saturation conditions during the saturation process. A calibrating solution with known resistivity was used to determine the geometric factor. Particle sizes were determined by sieving and the pipette method, using $Na_4P_2O_7$ as a dispersant (Klute, 1986, p. 393, 399–404, but with the sand-silt boundary at 0.063 mm).

Brunet et al. (2010) described remarkable conductivity increases of water with low initial mineralization, due to contact with the soil matrix. This may cause variation of resistivity with time. To minimize this effect we used spring water with high conductivity (approx. $\delta_{w25} = 150\,\mu S\,cm^{-1}$ for $T = 25\,^{\circ}C$). This corresponds to the mean conductivity of soil water in the study area, which is influenced by long-term contact with the subsoil.

Aside from the invariant parameters F_Θ and n_Θ, the resistivity of the pore water must be known to calculate the water content from resistivity values. Because it was not possible to extract pore water under dry conditions in summer, only a few measurements of pore water conductivity could be carried out in late spring and early autumn. To calculate water content from resistivity obtained by field surveys, the median value over the entire time period of ρ_w for each depth was used (cf. Table 2). Interim values between the extraction depths were linearly interpolated.

After reforming Eq. (1), it is possible, with known parameters F_Θ and n_Θ, and measured variables ρ_{eff} and ρ_w, to calculate volumetric water content:

$$\frac{\rho_{eff}}{F_\Theta \rho_w}^{\frac{1}{-n_\Theta}} = \Theta. \quad (2)$$

As water saturation (S) is defined as the ratio between water content and porosity (Φ), it is also possible to calculate the degree of saturation using:

$$\frac{\rho_{eff}}{F_\Theta \rho_w}^{\frac{1}{-n_\Theta}} \frac{1}{\Phi} = S. \quad (3)$$

HESSD
11, 5859–5903, 2014

2.4 Field work

2.4.1 Mapping

In addition to conventional percussion drilling, at the end of October 2008 we measured 7 ERT profiles to survey the subsurface resistivity distribution (Fig. 1A–G). A and C are parallel to the slope inclination of approx. 9°, connecting inflection points of contour lines. B, D, E, F, and G are perpendicular to these profiles (∠ A102.5°, ∠ B90°). This arrangement allows identifying potential 3-D-effects, which may cause inaccurate interpretation of the subsurface resistivity distribution. To improve the mapping results aided by hydrometric data, the profiles were located close to the tensiometer stations (distance < 2 m). For all resistivity measurements, a Lippmann 4 Point light hp instrument with 50 electrodes was used. Because of the expected heterogeneities (e.g. by roots or clasts) and the multiple layered stratification of periglacial cover beds, a Wenner-α array was found to be the most suitable configuration for the study area. This is characterized by low geometric factors (K), a high vertical resolution for laterally bedded subsurface structures, and a good signal-to-noise ratio (Dahlin and Zhou, 2004). To improve the spatial resolution, a Wenner-β array was measured additionally. With an electrode spacing of 1 m, this results in a combined dataset with 784 data points for each pseudo-section with a maximum depth of investigation of 9.36 m (Wenner-β: depth of investigation for radial dipole in homogeneous ground 0.195L according to Roy and Apparao, 1971; Apparao, 1991; Barker, 1989).

2.4.2 Monitoring

Time lapse measurements were performed with the same equipment, electrode array and spacing used for the mapping. The two time lapse profiles are congruent with profile A and B (cf. Fig. 1).

From May to December 2008, twenty seven time lapse measurements were carried out within almost weekly intervals.

HESSD
11, 5859–5903, 2014

To compare time lapse measurements and to apply sophisticated inversion routines, the location of electrodes needs to remain constant. For current injection we used stainless steel electrodes (diameter = 6 mm, length = 150 mm), completely plunged into the ground, thus avoiding shifting of electrodes, except for natural soil creep.

Subsoil temperature, especially in the upper layers, is characterized by distinct annual and daily variations. Therefore, temperature dependence of resistivity must be considered when comparing different time steps.

The installed tensiometers are able to measure soil temperature simultaneously. These data have been used to correct resistivity measurements to a standard temperature. Comparing several existing models for the correction of soil electrical conductivity measurements, Ma et al. (2011) conclude that the model (Eq. 4) as proposed in Keller and Frischknecht (1966), is practicable within the temperature range of environmental monitoring.

$$\rho_{25} = \rho_t (1 + \delta (T - 25\,^{\circ}\mathrm{C})) \quad (4)$$

With this equation the inverted resistivity (ρ_t) at the temperature (T) was corrected to a resistivity at a soil temperature of 25 °C (ρ_{25}). The empirical parameter δ is the temperature slope compensation, with $\delta = 0.025\,^{\circ}\mathrm{C}^{-1}$ being commonly used for geophysical applications (Keller and Frischknecht, 1966; Hayashi, 2004; Ma et al., 2011).

For inversion of the ERT data, we used the BERT Code (Günther et al., 2006). In order to account for the present topography, we applied an unstructured triangular discretization of the surface.

To calculate changes in resistivity, there are three different methodical approaches: either inverting the models for each point in time separately and subtract after inversion, to use the initial model as reference model for the time step, or inverting the differences of the two data sets (Miller et al., 2008). With our data, each method generates insufficient results with unsubstantiated artifacts. Changes have been calculated, which cannot be explained or related to any natural process. Descloitres et al. (2003, 2008b) showed with synthetic data that time lapse inversion may produce artifacts,

HESSD
11, 5859–5903, 2014

especially due to changes caused by shallow infiltration (decrease of resistivity), as mostly expected in our case.

The inversion had to be adjusted in order to minimize these artifacts. The expedient results were achieved by using the second approach with different inversion parameters for the initial reference model and each subsequent time lapse inversion. The first time step was calculated with smoothness constraints of 1st order and regularization strength $\lambda = 30$. The result was used as a reference model for the next time step. The following model was calculated with the antecedent time step as reference model, a chosen constraint minimum length, and higher regularization strength ($\lambda = 100$). By using this approach with each model as reference model for the next time step and adapting the inversion parameter, we could reduce the artifacts and achieve conclusive results. In our case this provides the best fit to the hydrometric data.

In order to find representative resistivity values as a function of depth, which are independent on small-scale heterogeneities, we subdivide the model down to a depth of 3 m into seven layers according to the boundaries of the described layering (cf. Table 1) and installation depth of hydrometric devices (cf. Fig. 1) (0–0.2, 0.2–0.4, 0.4–0.9, 0.9–1.2, 1.2–1.5, 1.5–2.0 and 2.0–3.0 m). The representative values are median resistivities in the layers from the stations H1a to H4a and H4b to H4a for profiles A and B, respectively.

2.5 Results

2.5.1 Hydrometry

During the period May to December 2008 the spring discharge varied between 0.07 and 1.67 $\mathrm{L\,s^{-1}}$. Median soil water tension of the study area, related to depth and time (cf. Fig. 2), indicates the impact of soil moisture on spring discharge. During summer increasing evapotranspiration causes the drying-out of soil. The spring showed only a slight reaction to precipitation events. Rainfall could only balance the soil water deficit and causes no runoff to the spring at most. Therefore, there is almost no runoff

HESSD
11, 5859–5903, 2014

generation in the summer season. Primarily base flow dominates and decreasing discharge is mainly caused by direct precipitation to the area surrounding the spring.

In contrast, during winter season (starting in November) at all depths lower tensions (< 90 hPa) were measured. Less evapotranspiration results in a replenishment of the storage water reservoirs in the subsurface. Due to the moist conditions, high presaturations predominate and cause a rapid runoff response with rain and the high discharges within the winter season.

Furthermore, there is an influence of the layered subsurface on soil moisture and runoff response. Until the beginning of May and again from December the low tensions of the upper LB indicate saturate conditions, in contrast to the deeper LB with higher tensions (cf. Fig. 2). Because of the anisotropic hydraulic properties, the percolation into deeper parts of LB is too slow, and the seepage water is accumulated in the LM and the upper LB. The backwater of the saturated depth range is mainly involved in runoff and causes strong interflow.

2.5.2 Laboratory

Within the separately analyzed samples, non-linear curve fitting was carried out. Using the method of least squares, the data could be fitted using a power function in the form of Archie's law (Eq. 1, $0.973 < r < 0.999$).

The exponent n_Θ shows a positive correlation to small grain sizes, primarily medium silt (6.3–20 µm, $r = 0.909$), but in the same case a negative correlation to grain sizes > 630 µm including clast content ($r = -0.852$) (cf. Fig. 3).

The amount of silt as well as the clast content are important distinctive attributes to differentiate the basal layer from the overlying intermediate or upper layer (Table 1). Two different "electrical" layers may be identified. This is due to the fact that the exponent is strongly influenced by grain size, which shows a remarkably change at the upper boundary of LB. On the other hand, grain size distribution and clast content are very similar between LH and LM, so that these may not be differentiated using ERT.

HESSD
11, 5859–5903, 2014

Figure 4 shows the aggregation of the single samples into two regions with different depth ranges.

The first depth range comprises the upper and the intermediate layer. These two periglacial layers are characterized by a high amount of silt (mostly medium silt) and comparatively low clast content. The exponent n_Θ ranges from 1.8 to 2.3. The second depth range is represented by the basal layer. This is characterized by a higher amount of coarse material at the expense of fine grain sizes. In this depth range n_Θ ranges from 0.7 to 1.8. Within each of these two depth ranges, we accept, analog to the properties of the substrate, similar electrical properties with a threshold at 0.9 m. The threshold depth of 0.9 m is not developed as an exact, continuous boundary. Rather it is a short transition zone, because the samples right from this depth may have properties of the shallow or the deeper region, similar to the geomorphological differentiation between the basal and intermediate layer, whose boundary varies between depths of 0.8 to 1 m. By combining samples from different depths into two regions, it was possible to derive the parameter for Eqs. (1)–(3) for each region (Table 3).

This relationship between water content and resistivity, shown in Fig. 4 and Table 3, is only a mean value for each depth range. In the first depth range (0–0.9 m), especially close to the surface, the differences in soil or electrical properties between the samples even at the same depth may vary. This higher variation may be explained by intense biotic activity near the surface, enhancing small-scale heterogeneity compared to deeper parts of the soil.

The fitted curves of both regions are quite similar, except for n_Θ. The formation factors are very similar (0.577 vs. 0.587, Table 3). With high saturation, the difference of resistivity between the depth ranges is small and primarily influenced by the conductivity of the pore fluid, but increases with decreasing water content. As a result of the higher exponent, LH and LM react more sensitively to water content changes than LB, especially at low presaturations. Related to this, small water content changes cause larger changes in resistivity than in the deeper region.

HESSD
11, 5859–5903, 2014

2.5.3 Mapping

At our study site the resistivity of the subsoil ranges from nearly 100 Ω m up to more than 4000 Ω m (cf. Fig. 5).

At the intersection between the longitudinal and diagonal profiles, a good match of the calculated resistivity models may be found at shallow depth. With increasing depth, the differences become more notable. To exclude potential errors (e.g. electrode positioning errors), the data quality may be evaluated by comparing normal and reciprocal measurements (LaBrecque et al., 1996; Zhou and Dahlin, 2003). For profile A and B repeated measurements with reciprocal electrode configuration were conducted. Thereby, no large errors (max ±1.2 %) could be found between normal and reciprocal measurements. Because of the absence of large potential errors, the increasing deviation with depth may be only explained by the inversion process, decreasing sensitivity, less spatial resolution or potential 3-D-effects.

The resistivity distribution of the subsurface is characterized by large-scale and small-scale heterogeneities, but also distinct patterns may be identified. At shallow depth up to 0.9 m, the study area is characterized by high resistivity. This comprises the upper and the intermediate layer.

Since the laboratory results indicate similar electrical properties, remarkable differences between upper and intermediate layers only occur, if water content deviates. There are areas, where the intermediate layer has higher resistivity, suggesting lower water content (cf. Fig. 6).

The hydrometric data show the driest conditions in 0.55–0.65 m (cf. Fig. 2), which is consistent with the high median resistivity of the intermediate layer at the time of data acquisition (cf. Fig. 7).

Resistivity decreases in greater depths (starting at 1 m). Thus, the basal layer is characterized by lower resistivity compared to the overlying layers. However, this is not constant in lateral direction. Two different patterns are found. In the “inner” area between the two depression lines (approx. between profile A and C), the resistivity of

HESSD
11, 5859–5903, 2014

the basal layer is lower than in the "outer" area (the hillsides) (cf. Fig. 7). Between the depression lines LB is characterized as a connected zone of low resistivity. A calculation of saturation using Eq. (3) and the porosity from Table 1 indicates that this may be interpreted as a connected saturated zone (Figs. 7 and 8).

Due to the slope gradient, water from the hillsides and upper parts of the catchment flows toward the depression lines, where it concentrates within the basal layer and forms a local slope groundwater reservoir. This results in a maximum decrease of resistivity in this zone as observed in all measured profiles at depths 1.5 to 4.5 m (cf. Fig. 8).

Percussion drilling confirmed that the thickness of LB downslope exceeds 3.5 m. Therefore, we assume that the entire saturated zone is located within the basal layer and since it is connected to the spring, it is also the source of the base flow.

This zone expands upslope, due to the fact that the depression lines diverge; the relief becomes smoother and does not show such strong recess (cf. Fig. 1). The water may easier spread laterally. On the other hand toward to the spring, it becomes more and more constricted. According to this, the shape of the surface may be partially transferred to the subsurface to identify regions of different hydrogeological conditions. Convex areas indicate dryer conditions in the basal layer in comparison to the concave or elongate parts of the hillslope, which may act as local aquifers.

It is not feasible to relate a specific resistivity to the underlying gneiss or its regolith. Percussion drilling was only realized down to 4 m depth where bedrock could not be reached. If the maximum thickness of the basal layer is equal to the saturated zone, as obtained by resistivity data, the change from basal layer to underlying gneiss may be set at a depth around 4.5 m.

ERT mapping of the spatial distribution of periglacial cover beds is associated with several restrictions. In our study area, stratification is concealed by the influence of pore water, the main factor driving resistivity. On the other hand this fact may be used to improve the understanding of the moisture conditions of the subsurface.

HESSD
11, 5859–5903, 2014

To check the equations obtained in the lab and also to compare directly with hydrometric data, we used the water contents from the ThetaProbes at H3a. Figure 9 compares water content, calculated with temperature-corrected resistivity ($\Theta_{\rho H3a}$ profile A close to H3A), with water content from the ThetaProbes (Θ_{Theta}) at time of mapping.

The values of $\Theta_{\rho H3a}$ and Θ_{Theta} show the same depth profile, but the values differ slightly. The resistivity depth profile shows a shift of −4.5 Vol% in comparison to the ThetaProbes. The different positions of the two probe locations could be one reason for this mismatch. Other reasons could be the inversion process of the resistivity data or differing pore water resistivity from the used median value (Table 2).

Because the data of the resistivity measurements and also the ThetaProbes may contain biased errors (e.g. caused by clast content or by the installation procedure), it is difficult to make reliable conclusions, which depth profile is more precise. However, despite of these slight differences both methods provide comparable results.

2.5.4 Monitoring

As the hydrometric data show, the first period from May to October was mainly characterized by drying of the subsurface. After that, humid conditions began to dominate (cf. Fig. 2). Major changes occur at shallow depth and proceed to depth, though remarkably attenuated. Each depth has its own characteristics, its own variation in time and shows different hydrological and electrical response. To better distinguish the results and to deal with the subsurface layered structure, a depth- or layer-based analysis is appropriate.

Figure 10 shows the trend of median resistivity for each depth range for the entire time series of profile A between H1a and H4a and profile B between H4b and H4a, in comparison with daily accumulated precipitation.

The resistivity of profile A clearly correlates with profile B (Table 4). This correlation is more pronounced at shallow depths. The absolute values are similar, except for the near-surface part of LH (0–0.2 m) and parts of LB (1.5–2.0 m). These two depth ranges have higher amounts at profile B than A at all points in time, due to the different

HESSD
11, 5859–5903, 2014

positions. Profile A is completely situated in one of the depression lines, in which moisture conditions can be expected in general.

During the measuring period, the upper layer (0–0.2 and 0.2–0.4 m) reacts with similar resistivity variations as the intermediate layer (0.4–0.9 m). Resistivity of the intermediate layer may temporarily exceed the upper layer (e.g. profile A October–December).

The temporal changes in resistivity decrease with depth. Short time variations are limited down to 2 m. Below, the differences are marginal with only a continuous slight increase during the investigated period.

The variation of resistivity is significant influenced by rainfall. As shown in Table 4, the upper and intermediate layers (< 0.9 m) show a strong negative correlation with the cumulated amount of precipitation (ppt). This correlation decreases with depth. Upper parts of the basal layer (0.9–1.5 m) respond slightly and delayed to intense rain events or enduring dry periods. Depths > 1.5 m show no direct correlation with rainfall. Water cannot infiltrate straight to greater depths because of decreasing hydraulic conductivity, evaporation, storage, or consumption of water by roots.

One problem is the temporal resolution. Because of the time intervals (usually ≥ 1 week), we are not able to resolve the entire temporal heterogeneity of the subsurface, which may lead to misinterpretation. For example, during the period from 3 to 16 September, the amount of 33 mm rain seems not to affect the resistivity of profile A. However, 32 of these 33 mm had already been fallen until 7 September. At profile B with an additional measurement on 9 September, resistivity at shallow depth decreases first and after that increases back to the initial level of 3 September (cf. Fig. 10b). Due to the missing time step, this alteration is not traced in profile A (cf. Fig. 10a).

This issue is also evident when comparing the resistivity with the soil suction data. With the higher temporal resolution of the tensiometer it is possible to resolve short time events e.g. single rain events (Fig. 2), which cannot be rendered with the resistivity survey (cf. Fig. 10).

During the investigation period, different trends could be identified. The initial conditions in April and early May are characterized by a highly saturated subsurface. This is

HESSD
11, 5859–5903, 2014

indicated by low soil water tension, high spring discharge, and high water content. Due to the humid conditions at the beginning of the measurements, the conductivity of the shallow subsurface is high and the observed resistivity is low relative to the seasonal variations.

A first annual trend covers the period between May and October. This period is mainly characterized by drying. The accumulated precipitation from 9 May to 21 October is only 337 mm. In combination with increasing evapotranspiration, this causes a mainstream drying of the subsurface (cf. Fig. 2). As a result of drying, at shallow depths (< 0.9 m) resistivity quickly increases until July. Below, the increase proceeds slightly, but continuously until October.

As mentioned above, resistivity, especially of LH and LM (up to 0.9 m), shows a high short time variability and is strongly associated with the amount of precipitation (ppt) (Table 4). During the investigated period three different response types could be identified that are exemplarily illustrated in Fig. 11 and compared to soil water tension.

1. A small amount of precipitation (cf. 23 September–7 October, ppt = 23 mm) causes a short deferment of increasing resistivity of LH and LM during the summer period. The values of initial state and time step are in the same order of magnitude. Within the temporal resolution, only a slight decrease could be recorded. Deeper parts are not affected and dry continuously. Constant discharge indicates that there is no runoff generation during this period. This amount of rain is only able to balance the deficit caused by evaporation at shallow depths, at least within the temporal resolution of measurements.

2. A medium amount of precipitation (cf. 1 July–15 July, ppt = 51.1 mm) causes a distinctive reaction at shallow depth. Resistivity at these depths shows a sharp decrease by comparatively the same ratio (~ 0.7). However, the signal is not traced into the deeper ground (> 1.2 m), which remains completely unaffected. So vertical seepage dominates in LH and LM, which leads to recharge of soil water. The water is predominantly fixed by capillary force; hence it does not percolate into

HESSD
11, 5859–5903, 2014

deeper layers. The short rise of discharge is caused by saturation overland flow in the spring bog.

3. A high amount of precipitation (cf. 22 October–4 November, ppt = 102.1 mm) results in a strong response down to 2.0 m and affects LH, LM as well as parts of LB. Such heavy rain period does not induce larger resistivity changes in LH and LM than the medium rain period, but influence deeper regions in the same order of magnitude as above. The water infiltrates to the upper, but does not reach the deeper basal layer (2–3 m). The vertical seepage is limited and therefore, the increasing spring discharge may only be caused by lateral subsurface flow, such as interflow in the unsaturated subsoil.

After the major rain event at the end of October, resistivity values remain low. Due to precipitation of 102.1 mm during the period from 19 November to 16 December, resistivity drops below the initial state and shows highly saturated conditions.

A comparison of water content obtained by ThetaProbes (Θ_{Theta}) and water content calculated from resistivity data for different depths over time at profile A 25 m near H3a ($\Theta_{\rho H3a}$) using Eq. (2), is shown in Fig. 12

At shallow depth (≤ 0.85 m), $\Theta_{\rho H3a}$ correlates closely with Θ_{Theta} (Table 5). However, there is a shift of the curves during the whole period. The volumetric water content from resistivity data is consequently smaller than from the ThetaProbes. In dry periods (e.g. July–October), the difference is less than under humid conditions (e.g. May).

In deeper parts the variations are attenuated. At a depth of 1.2 m there is almost no response over the year, until the heavy rain period at the end of October.

In 1.5 m depth the response of the ThetaProbes is marginal until December, but thereafter they show an increase. In contrast, $\Theta_{\rho H3a}$ shows already in late October a reaction to the heavy rain event, which is not reproducible with the ThetaProbes.

The same holds true for the correlation between resistivity (ρ_{H3a}) and soil suction at H3a (Ψ_{H3a}) (cf. Table 5). The resistivity of LH and LM fits well to the tensiometer data at the same depth, but in deeper parts it deviates.

HESSD
11, 5859–5903, 2014

These deviations between resistivity data and hydrometric measurements may have different causes. Both methods contain measuring errors, just as the laboratory and other hydrometric (e.g. soil–water resistivity) measurements. Furthermore, the ThetaProbes and Tensiometers measure punctual values. Heller (2012) demonstrated with dye infiltration experiments, that preferential flow is an important process in our study area. Hence, hydrometric point measurements may over- or underestimate soil moisture, depending on whether they are inside or outside a preferential pathway. Therefore the data are very limited, with restricted validity for the entire depth range or layer. In contrast, ERT has the advantage to integrate over a larger measuring volume, which makes it more suitable for extensive depth-related interpretations. Further, with high resolution ERT it is possible to identify small-scale heterogeneities such as preferential flow pathways.

3 Conclusions

In drainage basins, hillslopes link precipitation to river runoff. Runoff components, different flow pathways, and residence times are mainly influenced by the properties of the hillslope, especially the shallow subsurface. The knowledge of these properties is one of the keys to characterize the runoff dynamics in catchments. According to this, we used ERT for mapping the spatial heterogeneity of the subsurface structure on a hillslope with particular focus on mid-latitude slope deposits (cover beds).

ERT lets us differentiate between LH and LM as one unit and LB as another. Like the intrinsic properties (e.g. sedimentological), LH and LM have very similar electrical characteristics. Therefore, they may only being distinguished with ERT, if water contents are different or change differently with time.

On the contrary, LB has its own electrical characteristics. The pedophysical relationship, with neglecting surface conductivity, shows equal formation factors to LH and LM, but different exponents. With the lower exponent, LB is characterized by lower resistivity at the same water content. Therefore, the resistivity of LB is lower in the entire

HESSD
11, 5859–5903, 2014

study area, which is further reinforced by the increasing mineralization of pore water with depth.

Moreover, from the results of field measurements and pedophysical parameter determination in the laboratory we could derive a noninvasive method for direct monitoring of seasonal changes in subsurface resistivity and its relationship to precipitation and soil moisture on the hillslope scale. In combination with commonly used hydrometric approaches, we improved our understanding of the allocation, distribution, and movement of water in the subsurface. Different amounts of precipitation affect the subsurface moisture conditions differently and accordingly different depths take part in runoff generation.

Because pore water (amount and conductivity) is the main driver for resistivity, we arrive at some comprehensive interpretations of the subsurface moisture conditions. The high resistivities of LH and LM indicate low water contents, whereas LB is divided into two different moisture zones. On the hillsides water saturation of LB is less than between the depression lines, where low resistivity shows high water saturation and implies a local slope groundwater reservoir.

During investigation time, temperature-corrected resistivity showed distinct seasonal variations due to changes in moisture conditions, primarily influenced by precipitation and evapotranspiration. Close to the surface, these variations are very evident and decline with increasing depth, mainly limited to a depth of 2 m. This primarily affects LH, LM, and the upper parts of LB, since it may be assumed that deeper parts are already saturated and changes are only possible due to changes in water conductivity.

In summer the subsurface continuously dries, starting at the surface and proceeding to depth. This drying is temporarily interrupted by precipitation. Penetration depth and intensity of the response strongly depend on the amount of precipitation. During periods with a small amount of precipitation, infiltration is limited to LH. There is no runoff generation, and greater depths remain unaffected, which leads after repeated occurrence to drier conditions within LM compared to LH. In contrast to this, a response caused by a medium amount of precipitation includes LM and a small increase

HESSD
11, 5859–5903, 2014

in spring discharge. The main source of this runoff is saturated overland flow from the surface surrounding the spring. With a high amount of precipitation, changes in resistivity point to vertical seepage down to 2 m. The spring discharge consequently shows the major runoff generation, caused by lateral subsurface flow within LH, LM, and the upper LB.

The results from ERT measurements show a strong correlation to the hydrometric data. The average resistivity response is congruent to the average soil tension data. Water content obtained with ThetaProbes shows similar variations as calculated from the closest ERT profile. Consequently, soil moisture on the hillslope scale may be determined not only by punctual hydrometric measurements, but also by noninvasive ERT monitoring, provided pedophysical relationships are known. A combination improves the spatial understanding of the ongoing hydrological processes and is better suitable to identify heterogeneities.

Cassiani et al. (2009) pointed out that a combination of geophysical and hydrometric data may be used for quantitative estimation of hillslope moisture conditions. Our study has shown that this may also be applied to mid-latitude hillslopes covered by periglacial slope deposits. Nevertheless, there are some restrictions requiring further improvements.

One shortcoming is the temporal resolution. Some hydrological responses especially at hillslopes may proceed very quickly. The major goal for further research should be to increase the temporal resolution of ERT measurements to at least trace single rain events. This could be realized with automated data acquisitions as described in Kuras et al. (2009).

Another aim should be to improve the spatial resolution. Since preferential flow is an important process, a high-resolution ERT in combination with additional cross-borehole measurements would be more suitable to deal with small-scale heterogeneities and to overcome the problem of decreasing sensitivity with depth.

Acknowledgements. We acknowledge support by the German Research Foundation and the Open Access Publication Funds of the TU Dresden.

HESSD
11, 5859–5903, 2014

References

AD-hoc AG-Boden: Bodenkundliche Kartieranleitung, 5th Edn., Bundesanst. für Geowiss. und Rohstoffe in Zusammenarb. mit den Staatl. Geol. Diensten, Hannover, 2005. 5861

Amoozegar, A.: A compact constant-head permeameter for measuring saturated hydraulic conductivity of the Vadose Zone, Soil Sci. Soc. Am. J., 53, 1356–1361, 1989. 5887

Anderson, M. G. and Burt, T. P. (Eds.): Process studies in hillslope hydrology, Wiley, Chichester, West Sussex, England, New York, 1990. 5861

Apparao, A.: Geoelectric profiling, Geoexploration, 27, 351–389, 1991. 5866

Archie, G.: The electrical resistivity log as an aid in determining some reservoir characteristics, T. Am. I. Min. Met. Eng., 146, 54–61, 1942. 5864

Barker, R.: Depth of investigation of collinear symmetrical four-electrode arrays, Geophysics, 54, 1031–1037, 1989. 5866

Bechtold, M., Vanderborght, J., Weihermueller, L., Herbst, M., Günther, T., Ippisch, O., Kasteel, R., and Vereecken, H.: Upward transport in a three-dimensional heterogeneous laboratory soil under evaporation conditions, Vadose Zone J., 11, doi:10.2136/vzj2011.0066, 2012. 5862

Beff, L., Günther, T., Vandoorne, B., Couvreur, V., and Javaux, M.: Three-dimensional monitoring of soil water content in a maize field using Electrical Resistivity Tomography, Hydrol. Earth Syst. Sci., 17, 595–609, doi:10.5194/hess-17-595-2013, 2013. 5862

Benderitter, Y. and Schott, J. J.: Short time variation of the resistivity in an unsaturated soil: the relationship with rainfall, Eur. J. Environ. Eng. Geophys., 4, 37–49, 1999. 5862

Binley, A., Henry-Poulter, S., and Shaw, B.: Examination of solute transport in an undisturbed soil column using electrical resistance tomography, Water Resour. Res., 32, 763–769, 1996a. 5862

Binley, A., Shaw, B., and Henry-Poulter, S.: Flow pathways in porous media: electrical resistance tomography and dye staining image verification, Meas. Sci. Technol., 7, 384–390, 1996b. 5862

Brunet, P., Clément, R., and Bouvier, C.: Monitoring soil water content and deficit using Electrical Resistivity Tomography (ERT) a case study in the Cevennes area, France, J. Hydrol., 48, 146–153, 2010. 5862, 5865

HESSD
11, 5859–5903, 2014

Cassiani, G., Bruno, V., Villa, A., Fusi, N., and Binley, A.: A saline trace test monitored via time-lapse surface electrical resistivity tomography, J. Appl. Geophys., 59, 244–259, 2006. 5862

Cassiani, G., Godio, A., Stocco, S., Villa, A., Deiana, R., Frattini, P., and Rossi, M.: Monitoring the hydrologic behaviour of a mountain slope via time-lapse electrical resistivity tomography, Near Surf. Geophys., 7, 475–486, 2009. 5862, 5879

Chifflard, P., Didszun, J., and Zepp, H.: Skalenübergreifende Prozess-Studien zur Abflussbildung in Gebieten mit periglazialen Deckschichten (Sauerland, Deutschland), Grundwasser, 13, 27–41, 2008. 5861

Dahlin, T. and Zhou, B.: A numerical comparison of 2-D resistivity imaging with 10 electrode arrays, Geophys. Prospect., 52, 379–398, 2004. 5866

Daily, W., Ramirez, A., LaBrecque, D. J., and Nitao, J.: Electrical resistivity tomography of vadose water movement, Water Resour. Res., 28, 1429–1442, 1992. 5862

De Morais, F., De Almeida Prado Bacellar, L., and Aranha, P. R. A.: Study of flow in vadose zone from electrical resistivity surveys, Rev. Bras. Geofis., 26, 115–122, 2008. 5862

Descloitres, M., Ribolzi, O., and Le Troquer, Y.: Study of infiltration in a Sahelian gully erosion area using time-lapse resistivity mapping, Catena, 53, 229–253, 2003. 5867

Descloitres, M., Ribolzi, O., Troquer, Y. L., and Thiébaux, J. P.: Study of water tension differences in heterogeneous sandy soils using surface ERT, J. Appl. Geophys., 64, 83–98, 2008a. 5862

Descloitres, M., Ruiz, L., Sekhar, M., Legchenko, A., Braun, J., Mohan Kumar, M. S., and Subramanian, S.: Characterization of seasonal local recharge using electrical resistivity tomography and magnetic resonance sounding, Hydrol. Process., 22, 384–394, 2008b. 5862, 5867

Di Baldassarre, G. and Uhlenbrook, S.: Is the current flood of data enough? A treatise on research needs for the improvement of flood modelling, Hydrol. Process., 26, 153–158, 2012. 5861

French, H. and Binley, A.: Snowmelt infiltration: monitoring temporal and spatial variability using time-lapse electrical resistivity, J. Hydrol., 297, 174–186, 2004. 5862

Garré, S., Koestel, J., Günther, T., Javaux, M., Vanderborght, J., and Vereecken, H.: Comparison of heterogeneous transport processes observed with electrical resistivity tomography in two soils, Vadose Zone J., 9, 336–349, 2010. 5862

HESSD

11, 5859–5903, 2014

Garré, S., Javaux, M., Vanderborght, J., Pages, L., and Vereecken, H.: Three-dimensional electrical resistivity tomography to monitor root zone water dynamics, Vadose Zone J., 10, 412–424, 2011. 5862

Günther, T., Rücker, C., and Spitzer, K.: Three-dimensional modelling and inversion of dc resistivity data incorporating topography – II. Inversion, Geophys. J. Int., 166, 506–517, 2006. 5867

Hayashi, M.: Temperature-electrical conductivity relation of water for environmental monitoring and geophysical data inversion, Environ. Monit. Assess., 96, 119–128, 2004. 5867

Heller, K.: Einfluss periglazialer Deckschichten auf die oberflächennahen Fließwege am Hang – eine Prozessstudie im Osterzgebirge, Sachsen, Ph.D. thesis, Faculty of Environmental Sciences, TU Dresden, available at: http://nbn-resolving.de/urn:nbn:de:bsz:14-qucosa-98437 (last access: 30 April 2014), 2012. 5861, 5863, 5877, 5893

Keller, G. V. and Frischknecht, F. C.: Electrical Methods in Geophysical Prospecting, Pergamon Press, Oxford, 1966. 5867

Kemna, A., Vanderborght, J., Hardelauf, H., and Vereecken, H.: Quantitative imaging of 3-D solute transport using 2-D time-lapse ERT: a synthetic feasibility study, in: 17th EEGS Symposium on the Application of Geophysics to Engineering and Environmental Problems, Colorado, USA, 342–353, 2004. 5862

Kirkby, M. J. (Ed.): Hillslope Hydrology, Wiley, Chichester, 1980. 5861

Kleber, A.: Lateraler Wasserfluss in Hangsedimenten unter Wald, in: Stoff- und Wasserhaushalt in Einzugsgebieten, Beiträge zur EU-Wasserrahmenrichtlinie, edited by: Lorz, C. and Haase, D., Springer Verlag, Heidelberg, 7–22, 2004. 5861

Kleber, A. and Schellenberger, A.: Slope hydrology triggered by cover-beds, With an example from the Frankenwald Mountains, northeastern Bavaria, Z. Geomorphol., 42, 469–482, 1998. 5861

Kleber, A. and Terhorst, B. (Eds.): Mid-Latitude Slope Deposits (Cover Beds), vol. 66 of Developments in sedimentology, 1st Edn., Elsevier, Amsterdam, Boston, Heidelberg, London, New York, Oxford, Paris, San Diego, San Francisco, Singapore, Sydney, Tokyo, 2013. 5861

Klute, A. (Ed.): Methods of Soil Analysis, Part 1: Physical and Mineralogical Methods, 2nd Edn., ASA, SSA, Madison, Wisconsin, 1986. 5865

Koestel, J., Kemna, A., Javaux, M., Binley, A., and Vereecken, H.: Quantitative imaging of solute transport in an unsaturated and undisturbed soil monolith with 3-D ERT and TDR, Water Resour. Res., 44, W12411, doi:10.1029/2007WR006755, 2008. 5862

HESSD
11, 5859–5903, 2014

Koestel, J., Vanderborght, J., Javaux, M., Kemna, A., Binley, A., and Vereecken, H.: Noninvasive 3-D transport characterization in a sandy soil using ERT: 1. Investigating the validity of ERT-derived transport parameters, Vadose Zone J., 8, 711–722, 2009a. 5862

Koestel, J., Vanderborght, J., Javaux, M., Kemna, A., Binley, A., and Vereecken, H.: Noninvasive 3-D transport characterization in a sandy soil using ERT: 2. Transport process inference, Vadose Zone J., 8, 723–734, 2009b. 5862

Kuras, O., Pritchard, J. D., Meldrum, P. I., Chambers, J. E., Wilkinson, P. B., Ogilvy, R. D., and Wealthall, G. P.: Monitoring hydraulic processes with automated time-lapse electrical resistivity tomography (ALERT), CR Geosci., 341, 868–885, 2009. 5879

LaBrecque, D. J., Miletto, M., Daily, W., Ramirez, A., and Owen, E.: The effects of noise on Occam's inversion of resistivity tomography data, Geophysics, 61, 538–548, 1996. 5871

Leslie, I. N. and Heinse, R.: Characterizing soil-pipe networks with pseudo-three-dimensional resistivity tomography on forested hillslopes with restrictive horizons, Vadose Zone J., 12, doi:10.2136/vzj2012.0200, 2013. 5862

Lesmes, D. P. and Friedman, S. P.: Relationships between the electrical and hydrogeological properties of rocks and soils, in: Hydrogeophysics, edited by: Rubin, Y. and Hubbard, S. S., Springer, Dordrecht, 87–128, 2006. 5862, 5864

Ma, R., McBratney, A., Whelan, B., Minasny, B., and Short, M.: Comparing temperature correction models for soil electrical conductivity measurement, Precis. Agric., 12, 55–66, 2011. 5867

Massuel, S., Favreau, G., Descloitres, M., Le Troquer, Y., Albouy, Y., and Cappelaere, B.: Deep infiltration through a sandy alluvial fan in semiarid Niger inferred from electrical conductivity survey, vadose zone chemistry and hydrological modelling, Catena, 67, 105–118, 2006. 5862

McDonnell, J. J.: Where does water go when it rains? Moving beyond the variable source area concept of rainfall–runoff response, Hydrol. Process., 17, 1869–1875, 2003. 5862

McDonnell, J. J., Tanaka, T., Mitchell, M. J., and Ohte, N.: Hydrology and biogeochemistry of forested catchments, Hydrol. Process., 15, 1673–1674, 2001. 5861

McDonnell, J. J., Sivapalan, M., Vaché, K., Dunn, S., Grant, G., Haggerty, R., Hinz, C., Hooper, R., Kirchner, J., Roderick, M. L., Selker, J., and Weiler, M.: Moving beyond heterogeneity and process complexity: a new vision for watershed hydrology, Water Resour. Res., 43, W07301, doi:10.1029/2006WR005467, 2007. 5861

HESSD
11, 5859–5903, 2014

Michot, D., Benderitter, Y., Dorigny, A., Nicoullaud, B., King, D., and Tabbagh, A.: Spatial and temporal monitoring of soil water content with an irrigated corn crop cover using surface electrical resistivity tomography, Water Resour. Res., 39, SBH 14-1–SBH 14-20, 2003. 5862

Miller, C. R., Routh, P. S., Brosten, T. R., and McNamara, J. P.: Application of time-lapse ERT imaging to watershed characterization, Geophysics, 73, G7–G17, 2008. 5862, 5867

Moldenhauer, K.-M., Heller, K., Chifflard, P., Hübner, R., and Kleber, A.: Influence of cover beds on slope hydrology, in: Mid-Latitude Slope Deposits (Cover Beds), edited by: Kleber, A. and Terhorst, B., vol. 66 of Developments in Sedimentology, Elsevier, Amsterdam etc., 127–152, 2013. 5861, 5887, 5899

Oldenborger, G. A., Knoll, M. D., Routh, P. S., and LaBrecque, D. J.: Time-lapse ERT monitoring of an injection/withdrawal experiment in a shallow unconfined aquifer, Geophysics, 72, F177–F188, 2007. 5862

Perri, M. T., Cassiani, G., Gervasio, I., Deiana, R., and Binley, A.: A saline tracer test monitored via both surface and cross-borehole electrical resistivity tomography: comparison of time-lapse results, J. Appl. Geophys., 79, 6–16, 2012. 5862

Popp, S., Altdorff, D., and Dietrich, P.: Assessment of shallow subsurface characterisation with non-invasive geophysical methods at the intermediate hill-slope scale, Hydrol. Earth Syst. Sci., 17, 1297–1307, doi:10.5194/hess-17-1297-2013, 2013. 5862

Ramirez, A., Daily, W., LaBrecque, D. J., Owen, E., and Chesnut, D.: Monitoring an underground steam injection process using electrical resistance tomography, Water Resour. Res., 29, 73–87, 1993. 5862

Robinson, D. A., Binley, A., Crook, N., Day-Lewis, F. D., Ferré, T. P. A., Grauch, V. J. S., Knight, R., Knoll, M. D., Lakshmi, V., Miller, R., Nyquist, J., Pellerin, L., Singha, K., and Slater, L.: Advancing process-based watershed hydrological research using near-surface geophysics: a vision for, and review of, electrical and magnetic geophysical methods, Hydrol. Process., 22, 3604–3635, 2008a. 5862

Robinson, D. A., Campbell, C. S., Hopmans, J. W., Hornbuckle, B. K., Jones, S. B., Knight, R., Ogden, F., Selker, J., and Wendroth, O.: Soil moisture measurement for ecological and hydrological watershed-scale observatories: a review, Vadose Zone J., 7, 358–389, 2008b. 5862

Robinson, D. A., Abdu, H., Lebron, I., and Jones, S. B.: Imaging of hill-slope soil moisture wetting patterns in a semi-arid oak savanna catchment using time-lapse electromagnetic induction, J. Hydrol., 416, 39–49, 2012. 5862

HESSD
11, 5859–5903, 2014

Roy, A. and Apparao, A.: Depth of investigation in direct current methods, Geophysics, 36, 943–959, 1971. 5866

Sauer, D., Scholten, T., and Felix-Henningsen, P.: Verbreitung und Eigenschaften periglaziärer Lagen im östlichen Westerwald in Abhängigkeit von Gestein, Exposition und Relief, Mitt. Dtsch. Bodenkdl. Ges., 96, 551–552, 2001. 5861

Scholten, T.: Periglaziäre Lagen in Mittelgebirgslandschaften – Verbreitungssystematik, Eigenschaften und Bedeutung für den Landschaftswasser- und stoffhaushalt, in: Tagungsbeiträge IFZ-Workshop Ressourcensicherung in der Kulturlandschaft, Selbstverlag, Justus-Liebig-Universität, Gießen, 11–15, 1999. 5861

Schön, J. H.: Physical Properties of Rocks: Fundamentals and Principles of Petrophysics, vol. 18 of Handbook of Geophysical Exploration: Seismic Exploration, Elsevier, Oxford, 2004. 5864

Singha, K. and Gorelick, S. M.: Saline tracer visualized with three-dimensional electrical resistivity tomography: field-scale spatial moment analysis, Water Resour. Res., 41, W05023, doi:10.1029/2004WR003460, 2005. 5862

Slater, L., Binley, A., Daily, W., and Johnson, R.: Cross-hole electrical imaging of a controlled saline tracer injection, J. Appl. Geophys., 44, 85–102, 2000. 5862

Tilch, N., Uhlenbrook, S., Didszun, J., Wenninger, J., Kirnbauer, R., Zillgens, B., and Leibundgut, C.: Hydrologische Prozessforschung zur Hochwasserentstehung im Löhnersbach-Einzugsgebiet (Kitzbüheler Alpen, Österreich), Hydrol. Wasserbewirts., 50, 67–78, 2006. 5862

Tromp-van Meerveld, H. J.: Hillslope hydrology: from patterns to processes, Ph.D. thesis, Oregon State University, Corvallis, 2004. 5861

Tromp-van Meerveld, H. J. and McDonnell, J. J.: Assessment of multi-frequency electromagnetic induction for determining soil moisture patterns at the hillslope scale, J. Hydrol., 368, 56–67, 2009. 5862

Uchida, T., McDonnell, J. J., and Asano, Y.: Functional intercomparison of hillslopes and small catchments by examining water source, flowpath and mean residence time, J. Hydrol., 327, 627–642, 2006. 5861

Uhlenbrook, S.: Von der Abflussbildungsforschung zur prozessorientierten Modellierung – ein Review, Hydrol. Wasserbewirts., 49, 13–24, 2005. 5862

HESSD
11, 5859–5903, 2014

Uhlenbrook, S., Didszun, J., and Wenninger, J.: Source areas and mixing of runoff components at the hillslope scale – a multi-technical approach, Hydrolog. Sci. J., 53, 741–753, 2008. 5861, 5862

Vanderborght, J., Kemna, A., Hardelauf, H., and Vereecken, H.: Potential of electrical resistivity tomography to infer aquifer transport characteristics from tracer studies: a synthetic case study, Water Resour. Res., 41, W06013, doi:10.1029/2004WR003774, 2005. 5862

Völkel, J., Leopold, M., Mahr, A., and Raab, T.: Zur Bedeutung kaltzeitlicher Hangsedimente in zentraleuropäischen Mittelgebirgslandschaften und zu Fragen ihrer Terminologie, Petermann. Geogr. Mitt., 146, 50–59, 2002a. 5861

Völkel, J., Zepp, H., and Kleber, A.: Periglaziale Deckschichten in Mittelgebirgen – ein offenes Forschungsfeld, Ber. deuts. Landesk., 76, 101–114, 2002b. 5861

Wenninger, J., Uhlenbrook, S., Tilch, N., and Leibundgut, C.: Experimental evidence of fast groundwater responses in a hillslope/floodplain area in the Black Forest Mountains, Germany, Hydrol. Process., 18, 3305–3322, 2004. 5861

Zhou, B. and Dahlin, T.: Properties and effects of measurement errors on 2-D resistivity imaging surveying, Near Surf. Geophys., 1, 105–117, 2003. 5871

Zhou, Q. Y., Shimada, J., and Sato, A.: Three-dimensional spatial and temporal monitoring of soil water content using electrical resistivity tomography, Water Resour. Res., 37, 273–285, 2001. 5862

HESSD

11, 5859–5903, 2014

Table 1. Properties of cover beds from the study site for an example profile – adapted from Moldenhauer et al. (2013).

Layer	Soil horizon	Color (moist)	Soil texture			Clasts (%)	bulk density (%)	porosity ($g\,m^{-3}$)	Hydraulic conductivity ($cm\,d^{-1}$)*
			Clay (%)	Silt (%)	Sand (%)				
LH	A/Bw	10YR/5/8	14	52	34	36	1.2	0.55	27
LM	2Bg	10YR/5/4	12	53	35	43	1.5	0.43	9
LB	3CBg	10YR/5/3	7	22	71	56	1.7	0.36	52

* Field-saturated hydraulic conductivity measured using the Compact Constant Head Permeameter (CCHP) method (Amoozegar, 1989).

HESSD
11, 5859–5903, 2014

Table 2. Median pore water conductivity σ_w and resistivity ρ_w per depth.

Depth [m]	0.3	0.6	0.85	1.05	1.65	2.3
σ_w [µS cm^{-1}]	72.4	107.8	111.6	114.7	135	156.7
ρ_w [Ω m]	138.1	92.8	89.6	87.2	74.1	63.8

HESSD
11, 5859–5903, 2014

Table 3. Fitted parameters for Eqs. (1)–(3) of the two different depth ranges.

Depth range	F_Θ	n_Θ	r
< 0.9 m	0.577	1.83	0.895*
≥ 0.9 m	0.587	1.34	0.888*

* $p < 0.01$

HESSD
11, 5859–5903, 2014

Table 4. Correlation between median resistivity of profiles A ($\rho_{\text{profile A}}$) and B ($\rho_{\text{profile B}}$) and between subsequent resistivity ratio of profile A ($\rho_{\text{timestep}}/\rho_{\text{initial}}$) and cumulative precipitation during the time step (ppt).

Depth [m]	$r_{(\rho_{\text{profile A}},\rho_{\text{profile B}})}$	$r_{(\frac{\rho_{\text{timestep}}}{\rho_{\text{initial}}},\text{ppt})}$
0–0.2	0.977[a]	−0.773[a]
0.2–0.4	0.988[a]	−0.770[a]
0.4–0.9	0.987[a]	−0.804[a]
0.9–1.2	0.987[a]	−0.586[a]
1.2–1.5	0.852[a]	−0.378[b]
1.5–2.0	0.831[a]	−0.078[b]
2.0–3.0	0.878[a]	0.173[b]

[a] $p < 0.01$
[b] $p > 0.01$

HESSD
11, 5859–5903, 2014

Table 5. Correlation of volumetric water content calculated from resistivity values (Θ_{H3a}) and water content from ThetaProbes (Θ_{Theta}) and correlation of resistivity at H3a (ρ_{H3a}) and soil suction at H3a (Ψ_{H3a}).

Depth [m]	$r_{(\Theta_{\rho H3a},\Theta_{Theta})}$	$r_{(\rho_{H3a},\Psi_{H3a})}$
0.30	0.863[a]	0.993[a]
0.55	0.957[a]	0.904[a]
0.85	0.885[a]	0.905[a]
1.20	0.136[a]	0.120[b]
1.50	0.619[a]	0.566[a]

[a] $p < 0.01$
[b] $p > 0.01$

HESSD
11, 5859–5903, 2014

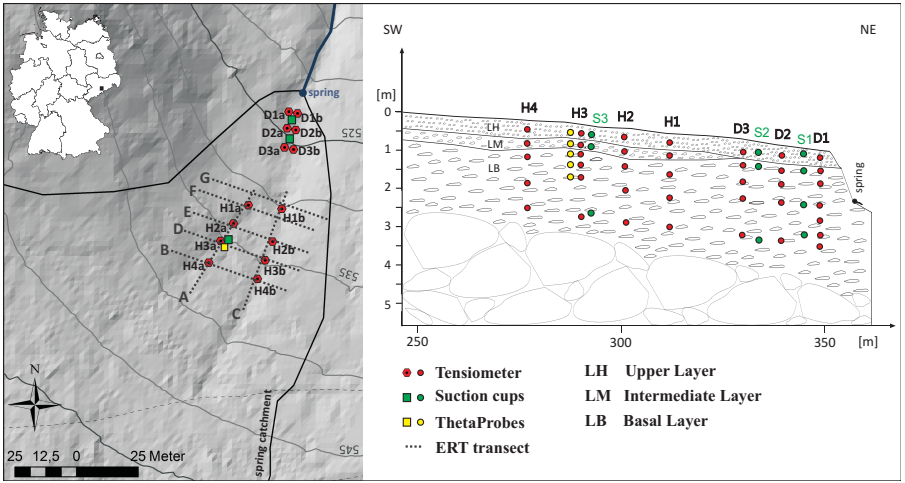

Figure 1. Study site with locations of ERT profiles and hydrometric stations (left panel) and profile section with installation depths of tensiometers, ThetaProbes and suction cups (right panel).

HESSD
11, 5859–5903, 2014

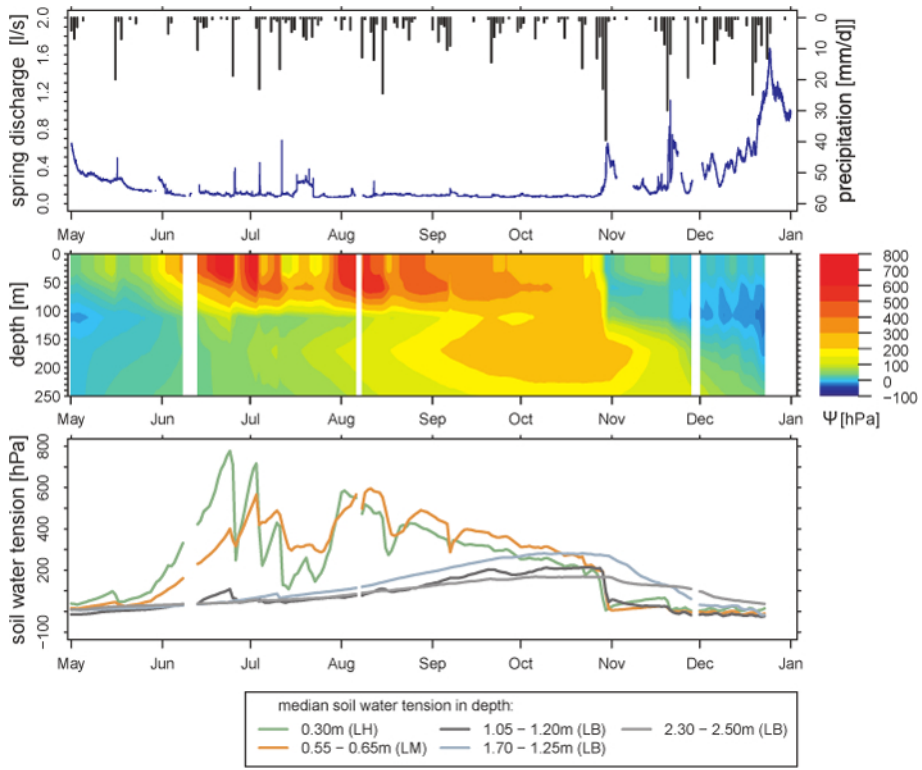

Figure 2. Spring discharge in comparison with daily precipitation (top panel), image of median soil water tension of the shallow subsurface (middle panel) and median soil water tension for different depths (bottom panel) – adapted from Heller (2012).

HESSD
11, 5859–5903, 2014

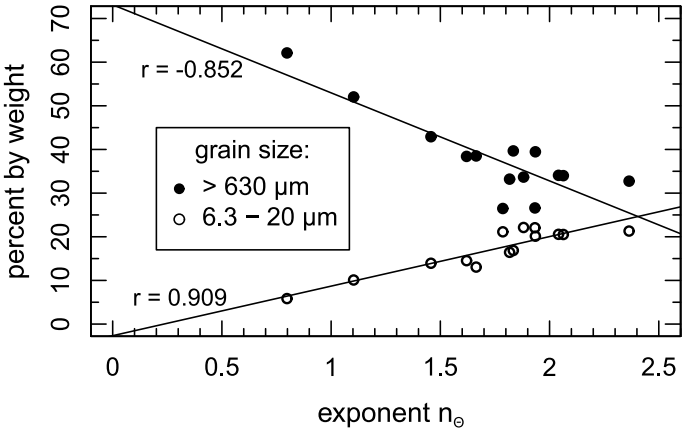

Figure 3. Exponent $n_{\ominus}$ in dependence of different grain sizes.

HESSD
11, 5859–5903, 2014

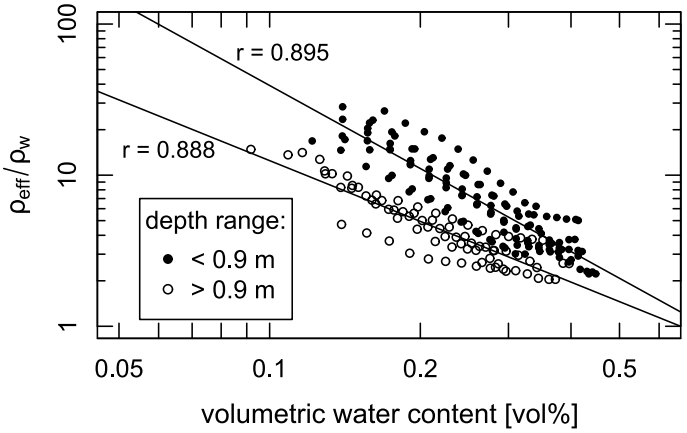

Figure 4. Volumetric water content in dependence of resistivity ratio (ρ_{eff}/ρ_w) for two different depth ranges.

HESSD
11, 5859–5903, 2014

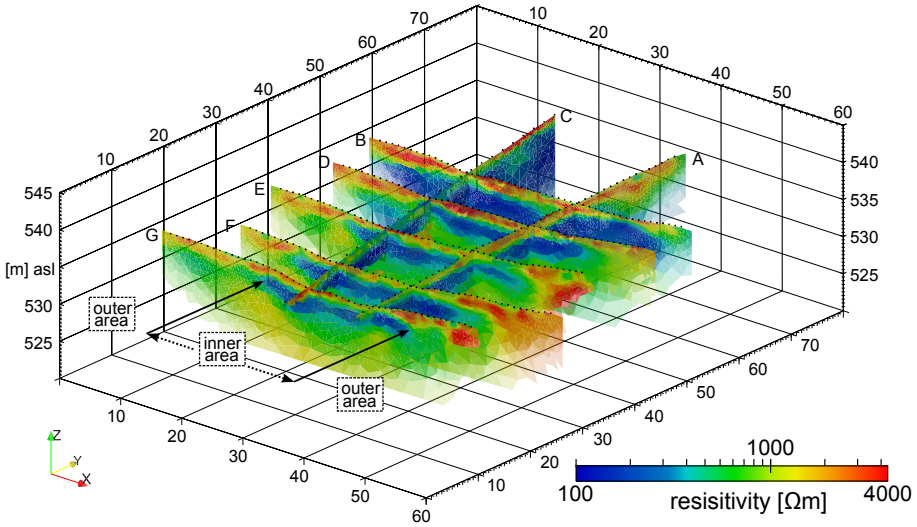

Figure 5. Resistivity results from ERT mapping (October 2008) of the study area: pseudo 3-D view of the profiles A to G.

HESSD
11, 5859–5903, 2014

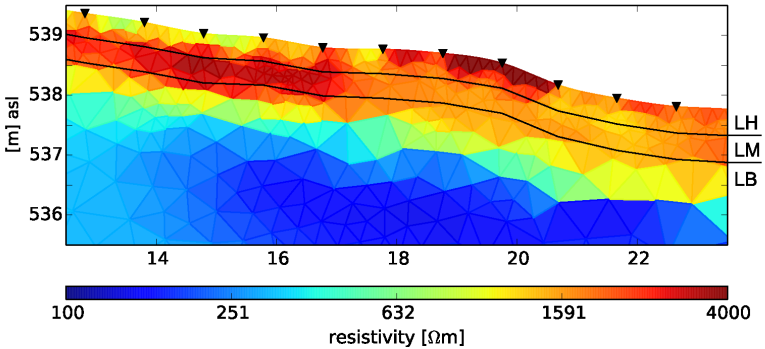

Figure 6. ERT section of profile A with plotted layer boundaries.

HESSD
11, 5859–5903, 2014

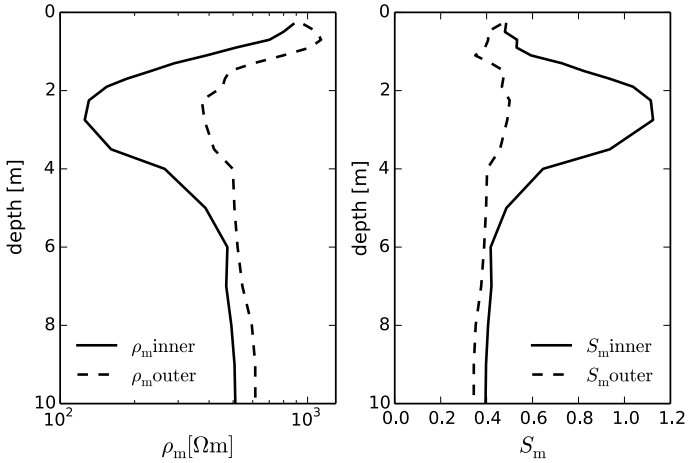

Figure 7. Median resistivity (left panel) and median water saturation (right panel) per depth for the inner region (between the depression lines) and outer region (hillslopes.)

HESSD
11, 5859–5903, 2014

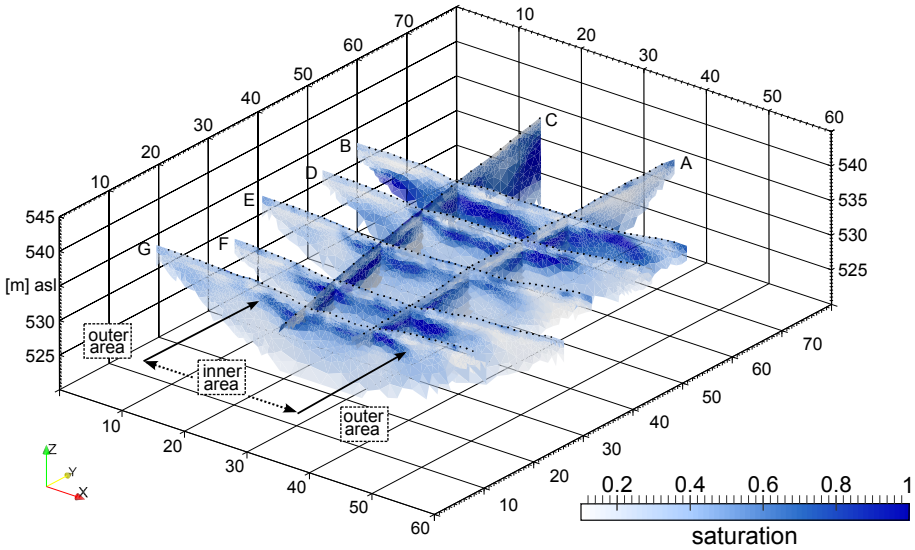

Figure 8. Calculated water saturation from resistivity data of the study site: pseudo 3-D view of the profiles A to G – adapted from Moldenhauer et al. (2013).

HESSD
11, 5859–5903, 2014

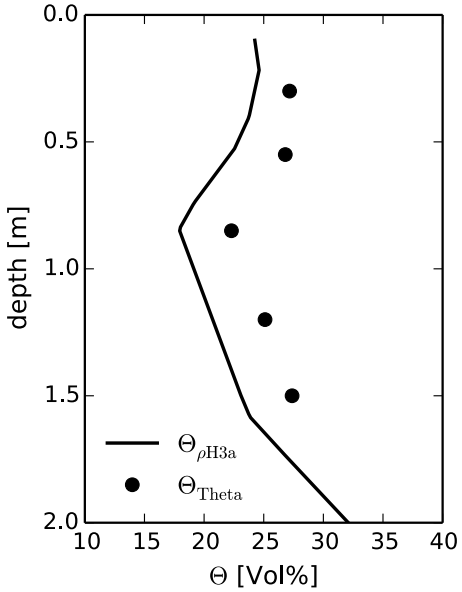

Figure 9. Volumetric water content calculated from resistivity data close to H3a in comparison with ThetaProbes at the time of the mapping.

HESSD
11, 5859–5903, 2014

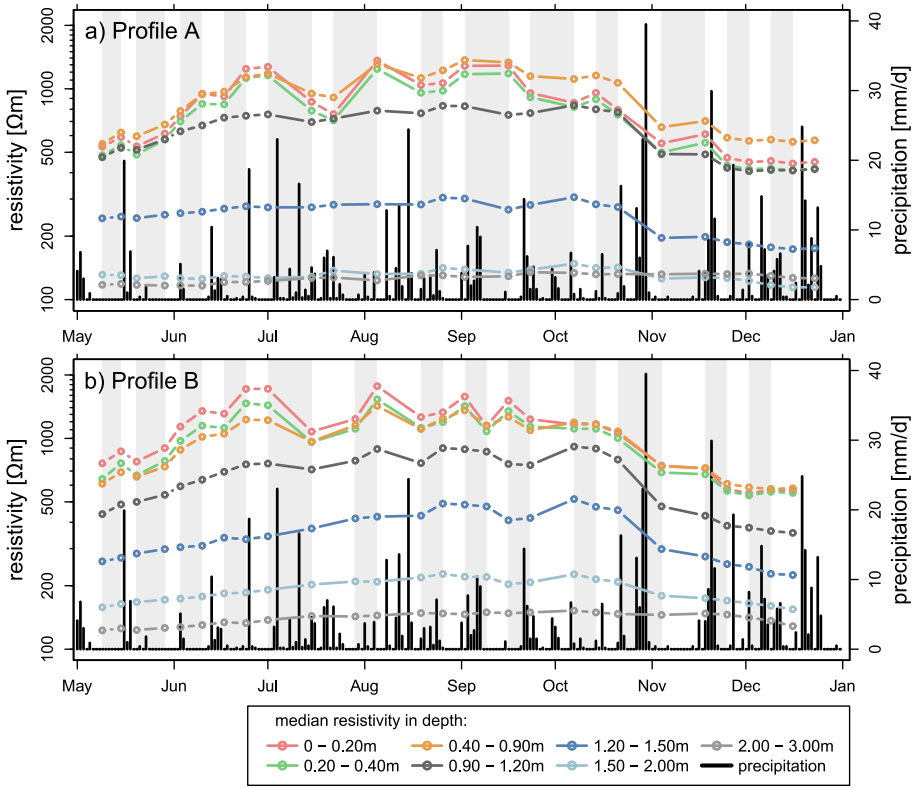

Figure 10. Trend of median resistivity for different depth ranges for **(a)** profile A and **(b)** profile B in comparison with daily precipitation.

HESSD
11, 5859–5903, 2014

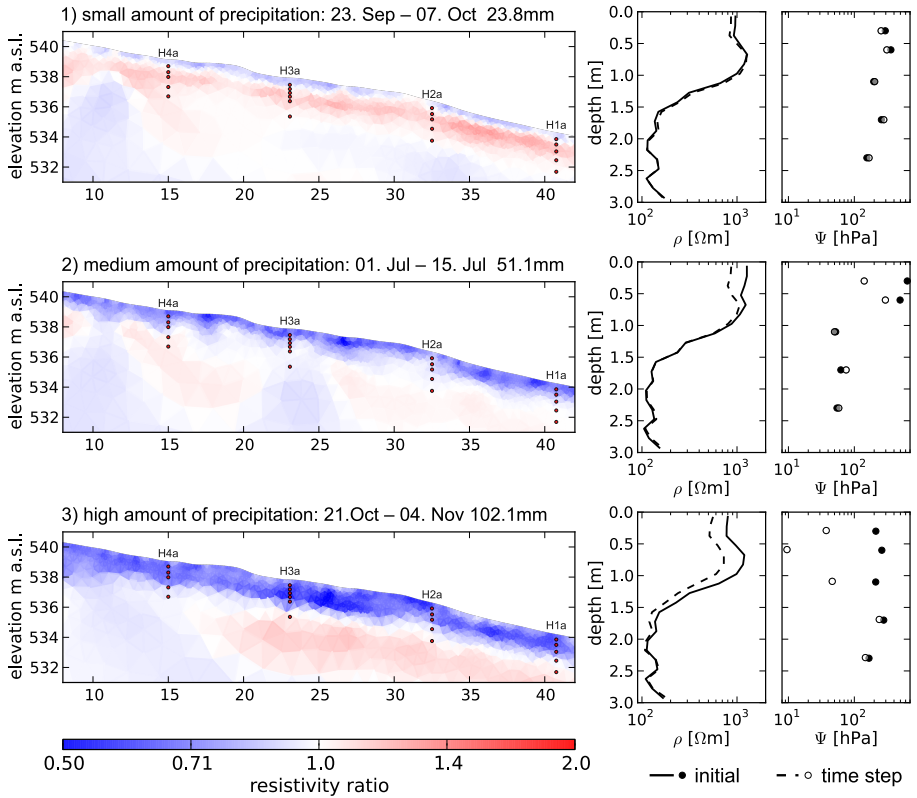

Figure 11. Ratio between subsequent resistivity (first column), median resistivity as a function of depth (second column) and median soil water tension (third column) for three exemplary precipitation responses: (1) small amount, (2) medium amount and (3) high amount.

HESSD
11, 5859–5903, 2014

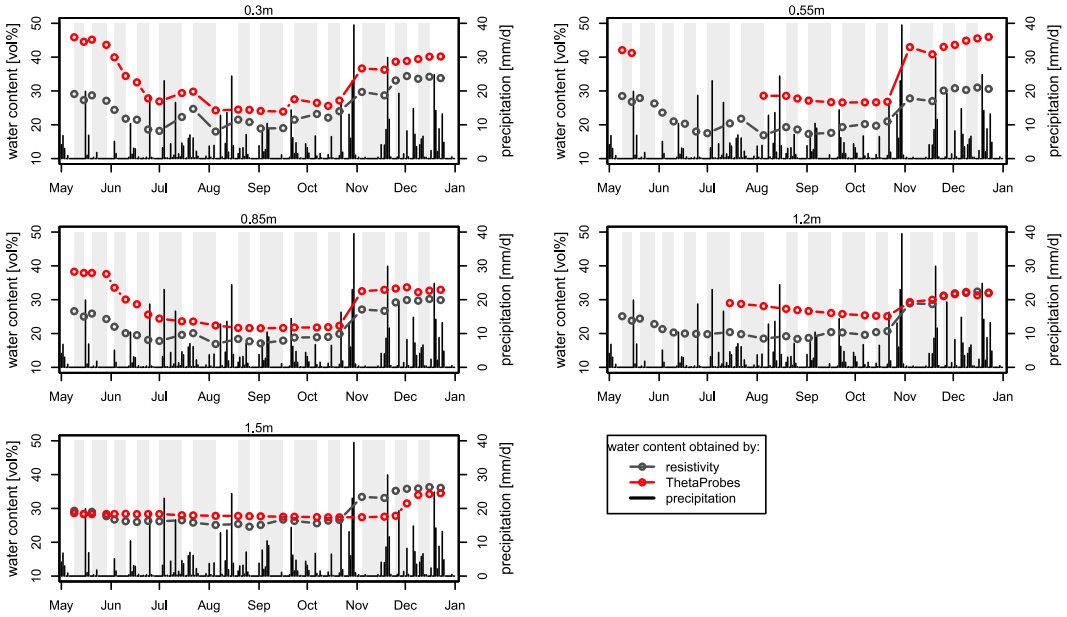

Figure 12. Trend of volumetric water content, obtained by resistivity data and ThetaProbes with daily precipitation for different depths.

HESSD
11, 5859–5903, 2014